Journal of Molecular Catalysis A: Chemical 335 (2011) 169–175

Contents lists available at ScienceDirect

Journal of Molecular Catalysis A: Chemical

journal homepage: www.elsevier.com/locate/molcata

Photocatalytic activity of $BiVO_4$ nanospheres obtained by solution combustion synthesis using sodium carboxymethylcellulose

U.M. García Pérez, S. Sepúlveda-Guzmán, A. Martínez-de la Cruz*, U. Ortiz Méndez

Facultad de Ingeniería Mecánica y Eléctrica, Universidad Autónoma de Nuevo León, Ciudad Universitaria, C.P. 66451, San Nicolás de los Garza, N.L., Mexico

ARTICLE INFO

Article history:
Received 23 June 2010
Received in revised form
17 November 2010
Accepted 27 November 2010
Available online 8 December 2010

Keywords:
$BiVO_4$
Heterogeneous photocatalysis
Template-directing agent

ABSTRACT

$BiVO_4$ nanospheres were obtained through solution combustion synthesis (SCS) in presence of sodium carboxymethylcellulose (CMC). The CMC polymer had a double function, as a fuel and as a protecting agent in the particles growth process. The formation and characterization of oxide was carried out by simultaneous thermal analysis (TGA/DTA), X-ray powder diffraction (XRD), scanning electron microscopy (SEM), Fourier transform infrared spectroscopy (FTIR), diffuse reflectance spectroscopy (DRS), and surface analysis (BET). The as-prepared $BiVO_4$ nanospheres calcined at 300 °C exhibited higher photocatalytic activity under visible-light irradiation than $BiVO_4$ samples prepared by coprecipitation and solid-state reaction methods in the degradation of rhodamine B (rhB). This behavior could be associated to their higher specific surface area (BET) and morphology. The analysis of the total organic carbon showed that the mineralization of rhB over a $BiVO_4$ photocatalyst is feasible (43% after 100 h of irradiation). A mechanism of formation of $BiVO_4$ nanospheres is also discussed.

1. Introduction

Since the discovery of heterogeneous photocatalysis [1], numerous efforts have been carried out to understand the mechanism of reaction and how to select the main variables that affect its efficiency. Several authors have associated the efficiency of a semiconductor photocatalyst with electronic, structural and morphological properties of the material such as the band gap energy (E_g), crystalline structure, surface area, and morphology. The possibility of controlling these variables is very interesting from a technological point of view because the development of materials with high photocatalytic activity allows their application to environmental fields such as wastewater treatment [2].

In the search of semiconductor materials with photocatalytic activity under visible-light irradiation, important efforts have been carried out in the last decade. For example, the TiO_2 anatase polymorph has been doped with nitrogen in order to increase its absorption in the visible range [3]. In another approach, several authors have proposed alternative oxides than traditional TiO_2 with high photocatalytic activity under visible-light irradiation such as $In_{1-x}Ni_xTaO_4$ [4], $CaIn_2O_4$ [5], $InVO_4$ [6], and $BiVO_4$ [7].

Among different studied oxides with activity under visible-light irradiation, $BiVO_4$ has received special attention. $BiVO_4$ crystallizes in three different polymorphs, i.e. tetragonal zircon, monoclinic distorted scheelite and tetragonal scheelite. Due to its relatively narrow band gap energy (2.4 eV), the monoclinic form exhibits the higher photocatalytic activity for chemical reactions induced with visible-light irradiation [8]. The photocatalytic activity of $BiVO_4$ has been recognized for the splitting reaction of water into hydrogen and oxygen [9,10], and for the degradation of organic dyes [11–13].

In order to improve the photocatalytic activity of the $BiVO_4$ monoclinic polymorph, different synthesis routes have been proposed in order to take a control of morphology and textural properties of the photocatalyst oxide. In this sense, besides the classical solid state reaction [14], monoclinic bismuth vanadate has been synthesized by means of layered vanadates in aqueous solution [7], sonochemistry [11], alkoxide methods [15], metal organic decomposition thin films [16], hydrothermal synthesis [17], coprecipitation [18], sol–gel [19], and hybrid organic–inorganic precursors [20].

Recently, the study of $BiVO_4$ oxide as photocatalyst has been focussed on the production of materials with a specific control of their 3D architecture morphology. For this purpose some additives has been incorporated in the synthesis route in order to act as template-directing reagent, chelating agent or surfactant agent, as is shown in the Table 1. The use of this type of additives leads to the formation of semiconductor oxides with remarkably improved photocatalytic properties. Among others methods, the use of water soluble polymers as templeate-directing agent during synthesis of nanostructures has increased in recent years.

In this work the sodium carboxymethylcellulose (CMC) is proposed as an additive during the $BiVO_4$ preparation. This polymer is a cellulose derivative obtained through the reaction between a

* Corresponding author. Tel.: +52 81 83 29 40 20; fax: +52 81 83 32 09 04.
E-mail address: azael70@yahoo.com.mx (A. Martínez-de la Cruz).

1381-1169/$ – see front matter © 2010 Elsevier B.V. All rights reserved.
doi:10.1016/j.molcata.2010.11.030

Table 1
Comparison of photcatalytic activity of $BiVO_4$ prepared by different synthesis routes in presence of organic additives.

Synthesis		Additive	Textural properties	Photocatalytic test	Reference
Aqueous method		DMA	Particles, 100–150 nm	rhB	[21]
	Microwave-assisted	CTAB	Nanostrips, widths ca. 10–30 nm and lengths ca. 2–3 μm	rhB and $O_2/AgNO_3$	[22]
	Ultrasonic-assisted	PEG 20000	Nanoparticles, ca. 60 nm, 12.0 $m^2 g^{-1}$	rhB	[23]
	Reflux	CTAB	Spherical, 400–700 nm, 1.8 $m^2 g^{-1}$	rhB	[24]
	Hard template	EG	Hollow spheres, outside Ø700 nm, 5.9 $m^2 g^{-1}$	rhB and CH_3CHO	[25]
Hydrothermal treatment	TMAH		Irregular particles, ca. 0.6 nm	–	[26]
	SDBS		Nanosheets, thickness 10–40 nm	rhB	[10]
	C12-MADS		Dendrite shape, length of the trunks of 2–6 μm and length of the branches 100–500 nm	rhB	[27]
	HTAB		Flower-like microclusters, Ø5–10 μm	MO	[28]
	CTAB		Flower-like structure, Ø1–2 μm; Lamellar structure, 0.08–0.12 μm, 0.3 $m^2 g^{-1}$	MO $O_2/Fe(NO_3)_3$	[29,30]
	SDS		Decahedral-like, 10 μm, 1.9 $m^2 g^{-1}$; Spherical particles, Ø ca. 5 μm	$O_2/AgNO_3$ –	[31,32]
	PEG 4000		Nanorods, Ø80–100 nm and length 25 μm, 9.1 $m^2 g^{-1}$	MB	[33]
	EDTA		Quasi-quadratic starlike, 1–2 μm, 1.1 $m^2 g^{-1}$	MB	[34]
	CTAB and PEG		Sheet-like structure, 0.4–1 μm	CO_2	[35]
Solution combustion synthesis	Urea		Dendrite shape, ca. 200–300 nm, 3.1 $m^2 g^{-1}$	Phenol and Cr(VI)	[36]
	Urea and citric acid		Spherical aggregated particles, Ø ca. 400–600 nm, 2.8 $m^2 g^{-1}$; Spherical aggregated particles, Ø ca. 150–500 nm, 2.6 $m^2 g^{-1}$	MB	[13,37]

DMA, N,N-dimethylacetamide; CTAB, cetyl trimethyl ammonium bromide; PEG, polyethylene glycol; EG, ethylene glycol; TMAH, tetramethyl ammonium hydroxide; SDBS, sodium dodecyl benzene sulfonate; C12-MADS, Gemini surfactant-monoalkylated disulfonated diphenyl oxide; HTAB, hexadecyl trimethyl ammonium bromide; SDS, sodium dodecyl sulfate; EDTA, ethylenediamine tetraacetic acid; rhB, rhodamine B; MO, methyl orange; MB, methylene blue.

cellulose alkali with sodium monochloroacetate. The CMC polymer has been gained interest due to its properties, such as polyelectrolytic nature, high ability to form complexes with divalent metal ions and high transparency in the UV and visible spectral regions [38]. These characteristics make of CMC a suitable stabilizer to control the particle size and morphology during the growing of metal oxide nanocrystals in aqueous solution. In addition, CMC can be easily removed from the resulting material due to its high water solubility or by low temperature treatments. To our best knowledge, the use of CMC as combustion source in the synthesis of $BiVO_4$ and its effect on the structural and photocatalytic properties of the resulting oxide have not been reported before.

In this work, nanospheres of $BiVO_4$ were prepared in presence of CMC by solution combustion synthesis (SCS). The influence of CMC in the morphology and textural properties of $BiVO_4$ oxide was analyzed. The effect of these variables in the photocatalytic activity of the oxide for the degradation of rhodamine B (rhB) under visible-light irradiation was also revised.

2. Experimental

2.1. Preparation of the $BiVO_4$ sample

$BiVO_4$ nanospheres were prepared by solution combustion synthesis in presence of sodium carboxymethylcellulose (CMC). The process involved in a first step the coprecipitation of a material containing stoichiometric amounts of Bi/V, followed by their ignition due to the combustion of the CMC. For this purpose, three aqueous solutions were prepared at 70 °C. In the first solution, 0.01 mol of $Bi(NO_3)_3{\cdot}5H_2O$ (Aldrich, 99%) were dissolved in 100 mL of 4 M HNO_3. The second solution was prepared by dissolving 0.01 mol of NH_4VO_3 (Productos Químicos Monterrey, 99%) in 100 mL of 2 M NH_4OH. The third solution was prepared by dissolving 1 g of CMC (Aldrich, 99%) in 50 mL of distilled water. The solutions of CMC and NH_4VO_3 were mixed under continuous stirring during 10 min. Afterwards, the bismuth nitrate solution was added dropwise to the vanadate-CMC solution with vigorous stirring. After mixing, the pH solution was adjusted at 9 by

using 2 M NH_4OH solution, getting a yellow suspension that was heated at 80 °C to promote the slow evaporation of the solvent. At this temperature, the sample was spontaneously ignited by effect of the thermal treatment when the solvent was totally removed. The yellow powder obtained after the combustion process was used as precursor for the $BiVO_4$ formation by following thermal treatments in air at 200, 300, and 450 °C (CMC-200, CMC-300, and CMC-450) for 24 h, respectively. In order to eliminate residues of reaction, i.e. by-products, samples were washed several times with distilled water. Likewise, for comparative purposes, $BiVO_4$ oxide was also synthesized by coprecipitation and solid-state reaction methods following the procedure described previously [39].

2.2. Sample characterization

Thermogravimetric and differential thermal analyses (TGA/DTA) of the precursor material were performed on a TA Instruments SDT Q600 thermal analyzer. The measurements were carried out under nitrogen atmosphere with a heating rate of 10 °C min^{-1}. The structural characterization of the samples was performed by X-ray powder diffraction using a Bruker D8 Advanced diffractometer with Cu Kα radiation, equipped with a Vantec high speed detector. The X-ray diffraction data were collected in the 2θ range 10–70° with a step scan rate of 0.05° 0.05 s^{-1}. The morphology of different samples was analyzed by scanning electron microscopy (SEM), using a FEI Nova Nanosem 200 field emission microscope.

The as prepared samples CMC-200, CMC-300, and CMC-450 were analyzed by Fourier transform infrared spectroscopy (FTIR) by using a PerkinElmer Spectrum spectrophotometer. This analysis was repeated after samples were washed several times with distilled water in order to determine the presence of reaction by-products. Specific surface area of the samples was evaluated by N_2 adsorption–desorption isotherms using a Bel-Japan Minisorp II Surface Area & Pore Size analyzer. The adsorption–desorption isotherms were measured at −196 °C after the pretreatment of the sample at 150 °C for 12 h. The UV-diffuse reflectance spectra of the samples were determined by using a UV–vis spectrophotometer equipped with an integration sphere (PerkinElmer Lambda 35). The residual organic carbon in the precursor, CMC-200, and CMC-300 samples was determined in a PerkinElmer Elemental Analyzer Serie II 2400.

2.3. Photocatalytic reaction

The photochemical reactor employed in this work consisted of a borosilicate glass beaker surrounded by a water-jacket to maintain the reaction temperature at 25 °C ± 1 °C. A Xe lamp of 6000 K with an illuminance of 1630 lx was used as visible-light source. The $BiVO_4$ photocatalytic activity was evaluated on the degradation reaction of rhB in water. In a glass beaker, 250 mL of rhB solution (5 mg L^{-1}) containing 250 mg of photocatalyst were put in ultrasonic bath for 10 min to eliminate aggregates. In order to achieve that adsorption–desorption equilibrium of the dye on the catalyst surface, the solution was kept in the dark for 1 h. After this time, the light source was turned on. During reaction, samples of 6 mL were taken at different time intervals and then separated through double centrifugation (4000 rpm, 20 min). The supernatant solution was decanted and the rhB concentration was determined through its absorption maximum band (554 nm) by using a UV–vis spectrophotometer.

The dye mineralization degree was monitored by analyzing the total organic carbon content (TOC) in the solutions with different irradiation times. Performing a typical experiment, 250 mL of a rhB solution (40 mg L^{-1}) containing 500 mg of photocatalyst was employed. The samples irradiated were analyzed in a Shimadzu VSCN8 TOC analyzer.

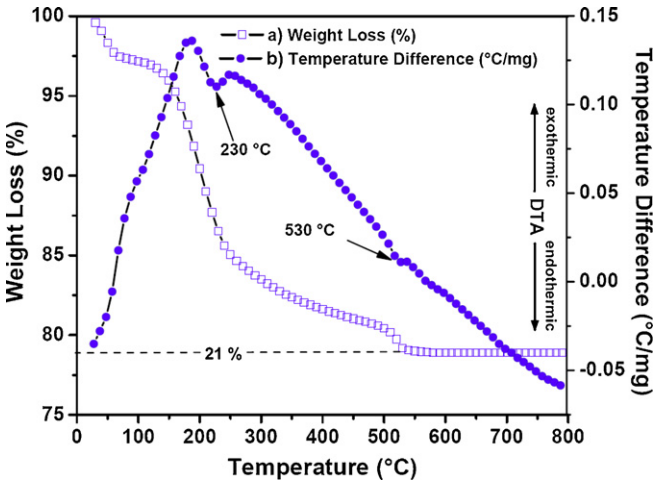

Fig. 1. TGA and DTA curves of the precursor used to prepare the $BiVO_4$ photocatalyst.

3. Results and discussions

3.1. Sample characterization

In the first step of the synthesis of $BiVO_4$ oxide, during the coprecipitation process at 80 °C, an orange powder was formed and precipitated. This temperature was kept in order to eliminate the solvent. When this process ended, a spontaneous and vigorous reaction took place due to the combustion process of CMC. The reaction was accompanied with a high energy delivery, and formation of a significant amount of white fumes. As result of the combustion process, the orange powder presented a color change from orange to yellow. The yellow powder will be identified hereafter as precursor.

The decomposition of the precursor to form $BiVO_4$ was followed by TGA/DTA simultaneous analysis, as it is shown in Fig. 1. An initial weight loss of 3% was observed at temperatures below 100 °C, which corresponds to the evaporation of adsorbed water on the precursor. An additional weight loss of 18% was observed between the range 100–530 °C and it corresponds to the elimination of water, nitrogen oxides and oxygen as decomposition products of the nitrates and ammonium salts. Two endothermic peaks were observed at 230 and 530 °C and were associated with these processes.

The formation of the $BiVO_4$ oxide was analyzed by X-ray diffraction at different stages of the precursor thermal treatments as it is shown in Fig. 2. This analysis revealed that the crystalline framework of the monoclinic $BiVO_4$ polymorph is formed after the combustion processes took place at 80 °C, according to the JCPDS Card No. 14-0688. Nevertheless, at this temperature the weight loss of the sample indicates that an important amount of different compounds not associated with $BiVO_4$ are also present. When the precursor was heated at 200 and 300 °C the X-ray diffraction pattern obtained corresponded with the formation of monoclinic form of $BiVO_4$. In both samples, the thermal treatment was carried out until the weight loss was constant. The amount of material lost, 20.65 and 20.55%, respectively, was similar to the value obtained by TGA analysis, i.e. 21%. A posterior thermal treatment at 450 °C leads to the formation of the $Bi_4V_2O_{11}$ oxide as an impurity. The formation of this oxide is common in the system Bi_2O_3–V_2O_5 by using similar temperatures [40]. Due to this result, only the samples obtained at 200 and 300 °C were used for photocatalytic studies.

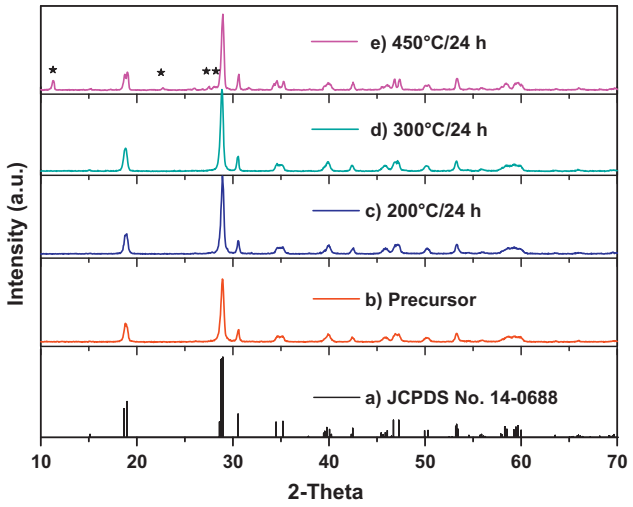

Fig. 2. XRD patterns of the as prepared samples of $BiVO_4$ and samples heated at different temperatures: (a) reference-JCPDS No. 14-0688, (b) precursor-80 °C, (c) 200 °C, (d) 300 °C, and (e) 450 °C (* diffraction lines associated with $Bi_4V_2O_{11}$).

Although the weight loss of the samples CMC-200 and CMC-300 revealed practically the total elimination of volatile material associated with the staring materials, it is possible that small amounts of reaction by-products remain in the samples. Fig. 3 shows the FTIR spectra of the $BiVO_4$ samples synthesized by SCS using CMC as fuel and protecting agent. The FTIR spectrum of CMC is also included for comparison (Fig. 3a). The FTIR spectrum of the precursor (Fig. 3b) shows an intense and broad band that includes the characteristic bands of $BiVO_4$ oxide; the symmetric and asymmetric stretching vibrations of V–O at 727 cm^{-1} and 833 cm^{-1}, and the bending vibration band of Bi–O at 678 cm^{-1}. Two additional bands at 1631 cm^{-1} attributed to O–H bending vibrations of water and at 1390 cm^{-1} assigned to NO_3^- vibrations were also observed. This suggests that NO_3^- anions remain on $BiVO_4$ surface as reaction by-product. The spectrum shows a lack of the characteristics bands of CMC, which implies that after combustion reaction, CMC was removed and possible combustion by-products were undetectable by FTIR analysis. The FTIR spectra of the samples obtained after thermal treatments at 200 and 300 °C show the characteristics bands of $BiVO_4$, and an additional stretching vibration band

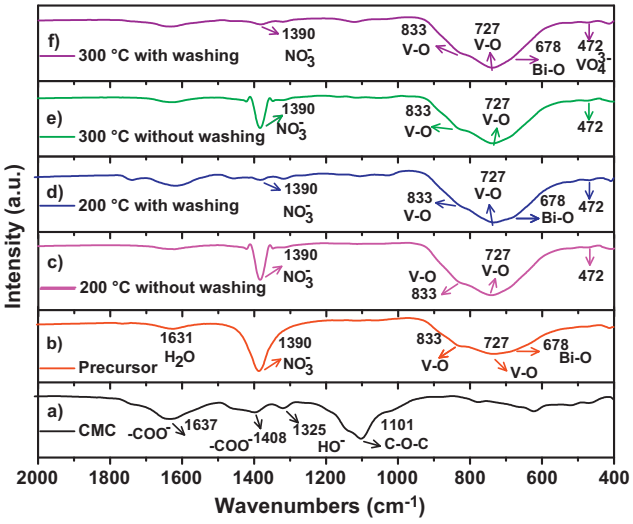

Fig. 3. FTIR spectra of the samples $BiVO_4$-CMC obtained at different temperatures, with and without distilled water washings.

of VO_4^{3-} at 472 cm^{-1} (Fig. 3c and e). However, the band associated with the NO_3^- vibration at 1390 cm^{-1} still remains strong, which shows that thermal treatments was inefficient to remove this type of by-product. $BiVO_4$ samples treated at 200 and 300 were then analyzed by FTIR after washing by repeated centrifugation and dispersion cycles in water. The resulting spectra showed the band at 1390 cm^{-1} considerably decreased (Fig. 3d and f). These results show that the thermal treatment and washing process can efficiently remove reaction by-products from the $BiVO_4$ samples.

The $BiVO_4$ samples synthesized by different thermal treatments were analyzed by SEM and the images are shown in Fig. 4. $BiVO_4$ sample obtained at 300 °C (Fig. 4c and d) consists of the aggregation of nearly spherical particles with particle size ranging from 50 to 200 nm. This morphology is comparable to that observed in the sample obtained at 200 °C (Fig. 4b); however, in the last case aggregation is more evident resulting in a globular morphology. This is possibly due to the thermal treatment at 200 °C was insufficient to remove completely the residues of CMC. This was confirmed when the carbon content was determined in the precursor, CMC-200, and CMC-300 samples. The amount of residual organic carbon was 0.33%, 0.08%, and 0.01%, respectively. Although such amounts of carbon are insufficient to be detected by FTIR, the difference observed by elemental analysis is the cause of the morphology developed by the particles. In this sense, the particle size of the aggregates is similar to that observed in the precursor (Fig. 4a). Whereas for the $BiVO_4$ sample obtained at 300 °C the organic material was removed revealing the morphology of the sample, this process was incomplete for the samples treated at 80 and 200 °C. This type of morphology has been observed in $BiVO_4$ samples where the synthesis was assisted by surfactants [23]. In addition, the residual organic material on $BiVO_4$ surface also avoided the unwanted particle growth during thermal treatments by a sintering process. The spherical morphology induced by the presence of CMC is very different to that observed by coprecipitation and solid-state reaction methods as shown in Fig. 4e and f. Note that the only difference between the combustion and coprecipitation synthesis was the addition of CMC in the first case.

Fig. 5 shows the proposed formation mechanism of $BiVO_4$ nanospheres by combustion synthesis in presence of CMC. The precursor was formed by the reaction between BiO^+ and VO_3^- ions when the respective solutions were mixed in presence of CMC polymer, producing an orange precipitate. The precipitate was crystalline due to the CMC combustion providing the energy required for the crystallization process. The spherical morphology was induced by the addition of CMC polymer that acts as stearic stabilizer. The resulting particles were encapsulated by the adsorption of CMC on the surface, which inhibited the disorder growth of the particles. The samples analyzed, after the combustion process, revealed the morphology in aggregates of granular particles. This morphology was more evident when the sample was treated at 300 °C, possibly due to the total elimination of residual organic material.

3.2. Photocatalytic reaction

The $BiVO_4$ photocatalytic activity was evaluated on the degradation of rhB in aqueous solution under visible-light irradiation. The evolution of the dye concentration during the photodegradation process by $BiVO_4$ is shown in Fig. 6. In order to evaluate the rhB grade of photolysis under visible-light irradiation, an additional experiment without photocatalyst was carried out. As it can be seen in Fig. 6, the rhB concentration was invariable all the time, which indicates that the combination of photocatalyst and light irradiation was necessary to degrade the dye from the solution. Data obtained with samples prepared by solid-state reaction and

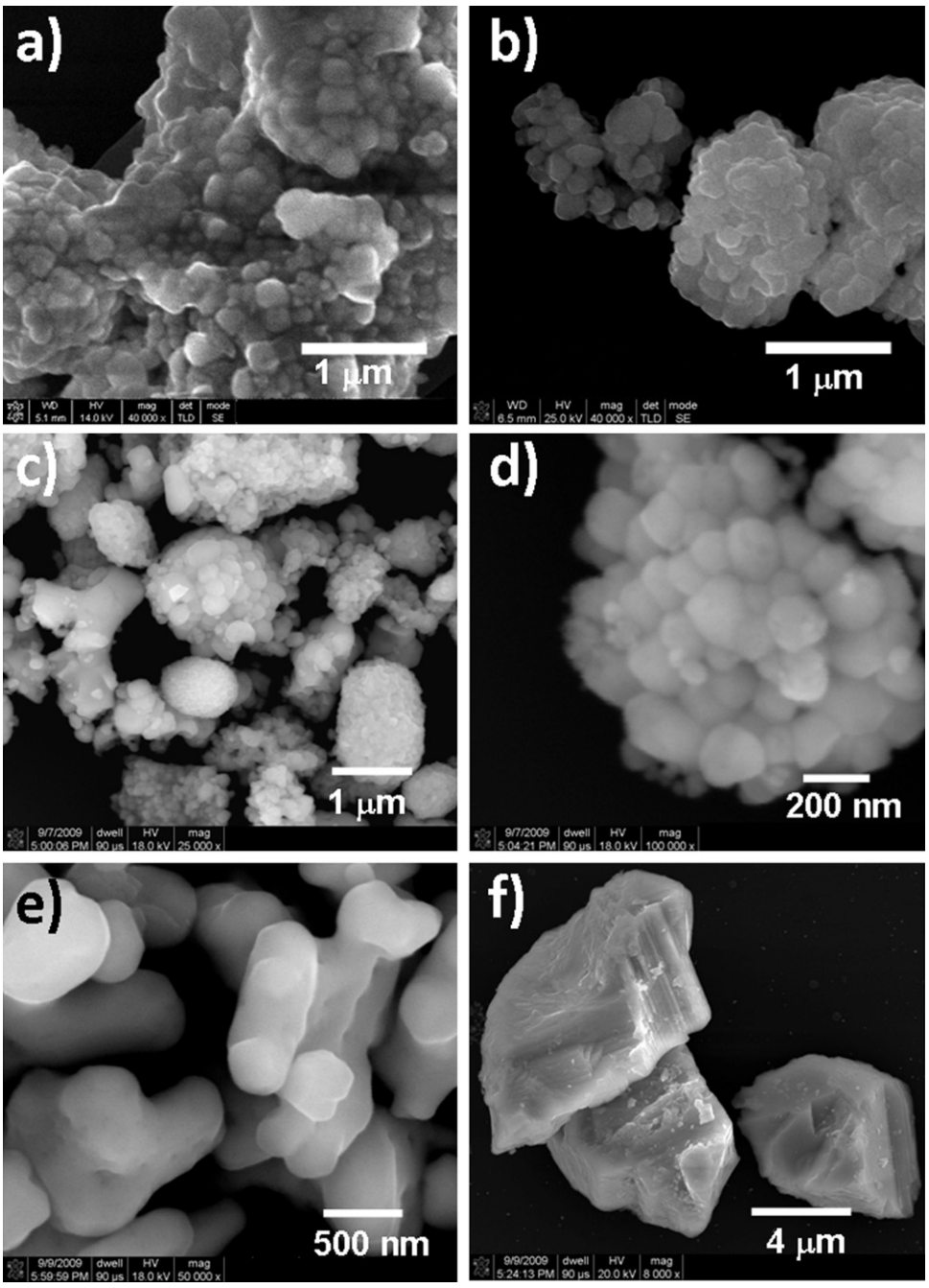

Fig. 4. SEM analysis of the morphology of $BiVO_4$ synthesized at different temperatures and synthesis methods: (a) precursor, (b) CMC-200, (c and d) CMC-300, (e) coprecipitation, and (f) solid-state reaction.

coprecipitation method free of CMC were also included for comparative purposes [39]. As can be seen, the presence of CMC during the formation of $BiVO_4$ nanoparticles promotes the formation of a material with a higher photocatalytic activity with respect to the sample synthesized by solid-sate reaction. In this sense, after 240 min of visible-light irradiation, the solution of rhB was bleached in a 20.4% when $BiVO_4$ obtained by solid-state reaction was used as photocatalyst. This amount was increased to 29.5% for the sample CMC-200. Nevertheless, improved results were observed in the sample prepared by conventional coprecipitation in absence of CMC. In similar period of time, the rhB solution was bleached in a 41.3%. An important increase of the photocatalytic activity was observed in the CMC-300 sample. In fact, after 180 min the rhB solution was bleached up to 100%. The cause of this increase in the photocatalytic activity cannot be explained only on the basis of the surface areas of the photocatalysts ($BiVO_4$-solid state reaction, 0.30 $m^2\,g^{-1}$; $BiVO_4$-coprecipitation, 1.50 $m^2\,g^{-1}$; $BiVO_4$-CMC200, 4.04 $m^2\,g^{-1}$; $BiVO_4$-CMC300, 3.00 $m^2\,g^{-1}$).

As it was described above, the presence of CMC during the synthesis of $BiVO_4$ promotes the formation of nanospheres due to the polymer matrix that inhibits the growth of the particles. This condition produces a more homogeneous morphology in the samples of $BiVO_4$-CMC than the observed in the coprecipitation method, and particles with higher surface area. Under this scheme, the spherical $BiVO_4$ nanoparticles seem to be more active in the photocatalytic degradation of rhB.

On the other hand, the difference in the photocatalytic activity observed in the $BiVO_4$-CMC samples can be associated with

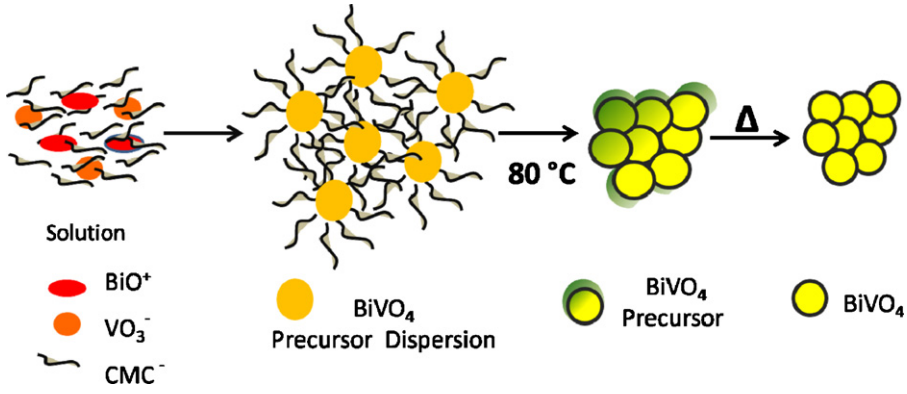

Fig. 5. Scheme of the formation of $BiVO_4$ nanospheres induced by the presence of CMC polymer.

the presence of residual organic material. According with the SEM micrographs in Fig. 4, the particles of the sample $BiVO_4$-CMC200 are embedded in a matrix due to the presence of residual organic material. When this material is removed, at 300 °C, more discrete particles were observed. The presence of residual organic material over the surface of the sample $BiVO_4$-CMC200 has a negative effect in the photocatalytic process. As it is well known, the organic dye should be adsorbed in the surface of $BiVO_4$ to the interchange of charges during the photocatalytic reaction. This adsorption takes place in the active sites of the oxide, which can be deactivated by the presence of residual organic material. This is the explanation why the sample $BiVO_4$-CMC300, with lower surface area, has a higher photocatalytic activity than $BiVO_4$-CMC200, with similar morphology but higher surface area. There is an enormous difference on the size of N_2 molecule employed on BET technique and the size of the molecule of rhB. Whereas the BET analysis revealed a true surface area, the adsorption of rhB can be affected by steric effects of the dye molecule on the interaction with the surface of photocatalyst. In a pioneer work, Graham described the adsorption process of methylene blue on activated carbons on the basis of the differences between the total surface area of the adsorbents and that accessible to methylene blue [41].

The kinetic data shown in Fig. 6 can be adjusted according to a first-order reaction equation, $\ln(C/C_0) = -k't$, where C_0 and C are the concentrations of rhB before and after the irradiation ($mg\,L^{-1}$), t the time (min) and k' is the apparent reaction rate constant (min^{-1}). On the basis of this model, the half-life time for bleaching of the rhB solution was $t_{1/2} = 78$ min for $BiVO_4$-CMC300. On the basis of this data, this sample has a photocatalytic efficiency 8 times higher than the sample synthesized by solid-state reaction, $t_{1/2} = 657$ min.

To determine the mineralization degree of the organic dye by $BiVO_4$-CMC300, TOC analyses were performed on dispersions with different irradiation times. In order to have more accuracy in the measurements performed in this experiment, an initial rhB concentration of 40 $mg\,L^{-1}$ was used. The dye mineralization degree was around 43% after 100 h of visible light irradiation. This result indicates that the rhB mineralization by the action of the $BiVO_4$-CMC300 photocatalyst is possible. This is an important point due to the fact that the complete de-ethylation of rhB leads to the solution bleaching, but not necessarily to the mineralization of the dye. The TOC experiments elucidate this point.

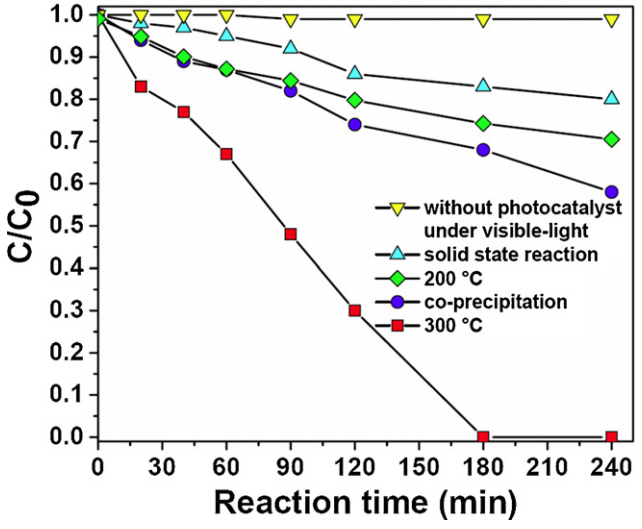

Fig. 6. Evolution of rhB concentration during its photocatalytic degradation in the presence of different samples of $BiVO_4$.

4. Conclusions

$BiVO_4$ oxide was synthesized by solution combustion synthesis in presence of sodium carboxymethylcellulose (CMC). The presence of the polymer promoted the formation of nanospheres with sizes ranged between 50 and 200 nm. The $BiVO_4$ nanospheres showed photocatalytic activity in the mineralization of rhodamine B under visible-ligth irradiation. The higher photocatalytic activity was observed in the sample treated at 300 °C, possibly due to the elimination of residual organic material producing more active sites in the surface of the photocatalyst.

Acknowledgements

We wish to thank to the Universidad Autónoma de Nuevo León (UANL) for its invaluable support through the project PAICYT 2009 and to CONACYT for supports the project 81546. We also thank to Departamento de Ecomateriales y Energía of Facultad de Ingeniería Civil (UANL) for its assistance on the materials characterization.

References

[1] K. Honda, A. Fujishima, Nature 238 (1972) 37.
[2] S. Malato, P. Fernández-Ibáñez, M.I. Maldonado, J. Blanco, W. Gernjak, Catal. Today 147 (2009) 1.
[3] S. Yang, L. Gao, J. Am. Ceram. Soc. 87 (2004) 1803.
[4] Z.G. Zou, J.H. Ye, K. Sayama, H. Arakawa, Nature 414 (2001) 625.
[5] J.W. Tang, Z.G. Zou, J.H. Ye, Chem. Mater. 16 (2004) 1644.
[6] Z. Zou, J. Ye, K. Sayama, H. Arakawa, Chem. Phys. Lett. 333 (2001) 57.
[7] A. Kudo, K. Omori, H. Kato, J. Am. Chem. Soc. 121 (1999) 11459.
[8] H. Jiang, H. Endo, H. Natori, M. Nagai, K. Kobayashi, J. Eur. Ceram. Soc. 28 (2008) 2955.
[9] K. Sayama, A. Nomura, T. Arai, T. Sugita, R. Abe, M. Yanagida, T. Oi, Y. Iwasaki, Y. Abe, H. Sugihara, J. Phys. Chem. B 110 (2006) 11352.
[10] A. Kudo, K. Ueda, H. Kato, I. Mikami, Catal. Lett. 53 (1998) 229.
[11] L. Zhang, D. Chen, X. Jiao, J. Phys. Chem. B 110 (2006) 2668.

[12] L. Zhou, W. Wang, S. Liu, L. Zhang, H. Xu, W. Zhu, J. Mol. Catal. A: Chem. 252 (2006) 120.
[13] H. Jiang, H. Endo, H. Natori, M. Nagai, K. Kobayashi, Mater. Res. Bull. 44 (2009) 700.
[14] T. Lu, B.C.H. Steele, Solid State Ionics 21 (1986) 339.
[15] K. Hirota, G. Komatsu, M. Yamashita, H. Takemura, O. Yamaguchi, Mater. Res. Bull. 27 (1992) 823.
[16] A. Galembeck, O.L. Alves, Thin Solid Films 365 (2000) 90.
[17] J.B. Liu, H. Wang, S. Wang, H. Yan, Mater. Sci. Eng. B 104 (2003) 36.
[18] P. Wood, F.P. Glasser, Ceram. Int. 30 (2004) 875.
[19] H. Liu, R. Nakamura, Y. Nakato, J. Electrochem. Soc. 152 (2005) G856.
[20] F. Rullens, A. Laschewsky, M. Devillers, Chem. Mater. 18 (2006) 771.
[21] L. Li, B. Yan, J. Alloys Compd. 476 (2009) 624.
[22] H.M. Zhang, J.B. Liu, H. Wang, W.X. Zhang, H. Yan, J. Nanopart. Res. 10 (2008) 767.
[23] M. Shang, W. Wang, L. Zhou, S. Sun, W. Yin, J. Hazard. Mater. 172 (2009)338.
[24] W. Yin, W. Wang, L. Zhou, S. Sun, L. Zhang, J. Hazard. Mater. 173 (2010) 194.
[25] W. Yin, W. Wang, M. Shang, L. Zhou, S. Sun, L. Wang, Eur. J. Inorg. Chem. (2009) 4379.
[26] M. Gotić, S. Musić, M. Ivanda, M. Šoufek, S. Popović, J. Mol. Struct. 744–747 (2005) 535.
[27] Y. Zheng, J. Wu, F. Duan, Y. Xie, Chem. Lett. 36 (2007) 520.
[28] A. Zhang, J. Zhang, Spectrochim. Acta Part A 73 (2009) 336.
[29] H. Li, G. Liu, X. Duan, Mater. Chem. Phys. 115 (2009) 9.
[30] D. Ke, T. Peng, L. Ma, P. Cai, K. Dai, Inorg. Chem. 48 (2009) 4685.
[31] T. Yang, D. Xia, G. Chen, Y. Chen, Mater. Chem. Phys. 114 (2009) 69.
[32] T. Yang, D. Xia, J. Cryst. Growth 311 (2009) 4505.
[33] F. Dong, Q. Wu, J. Ma, Y. Chen, Phys. Status Solidi A 206 (2009) 59.
[34] S. Sun, W. Wang, L. Zhou, H. Xu, Ind. Eng. Chem. Res. 48 (2009) 1735.
[35] Y. Liu, B. Huang, Y. Dai, X. Zhang, X. Qin, M. Jiang, M.-H. Whangbo, Catal. Commun. 11 (2009) 210.
[36] B. Xie, H. Zhang, P. Cai, R. Qiu, Y. Xiong, Chemosphere 63 (2006) 956.
[37] H. Jiang, M. Nagai, K. Kobayashi, J. Alloys Compd. 479 (2009) 821.
[38] A.H. Basta, H. El-Saied, Carbohyd. Polym. 74 (2008) 301.
[39] A. Martínez-de la Cruz, U.M. García Pérez, Mater. Res. Bull. 45 (2010) 135.
[40] K. Shantha, G.N. Subbanna, K.B.R. Varma, J. Solid State Chem. 142 (1999) 41.
[41] D. Graham, J. Phys. Chem. 59 (1956) 896.